J. Membrane Biol. 165, 175–181 (1998)

The Journal of
Membrane
Biology

The Functional Surface Charge Density of a Fast K Channel in the Myelinated Axon of *Xenopus laevis*

F. Elinder, P. Århem
The Nobel Institute for Neurophysiology, Department of Neuroscience, Karolinska Institutet, S-171 77 Stockholm, Sweden

Received: 11 December 1997/Revised: 24 April 1998

Abstract. The action of Mg^{2+} on the putative xKv1.1 channel in the myelinated axon of *Xenopus laevis* was analyzed in voltage clamp experiments. The main effect was a shift in positive direction of the open probability curve (16 mV at 20 mM Mg^{2+}), calculated from measurements of the instantaneous current at Na reversal potential after 50–100 msec steps to different potentials. The shift was measured at an open probability level of 25% to separate it from shifts of other K channel populations in the nodal region. The results could be explained in terms of screening effects on fixed charges located on the surface of the channel protein. Using the Grahame equation the functional charge density was estimated to $-0.45\ e\ nm^{-2}$. Analyzing this value, together with previously estimated values from other K channels, with reference to the charge of different extracellular loops of the channel protein, we conclude that the loop between the transmembrane S5 segment and the pore forming P segment determines the functional charge density of voltage-gated K channels.

Key words: Myelinated axon — Voltage clamp — K channels — Surface charges — Magnesium

Introduction

The shift of voltage-dependent gating of ion channels by divalent and trivalent cations (Frankenhaeuser & Hodgkin, 1957; Chandler, Hodgkin & Meves, 1965) has partly been explained by a screening of fixed membrane surface charges according to the Gouy-Chapman theory (for a review *see* McLaughlin, 1989; for binding effects *see* e.g., Cukierman, 1993, and Elinder & Århem, 1994*a*,*b*). A key question is where these charges are located. In principal they may be located on the lipid bilayer, on the carbohydrate chains attached to the channel protein or on the channel protein itself.

Both theoretical and experimental evidence seem to exclude the lipid bilayer as location. The Debye length of a charge in frog Ringer is short in comparison with the dimensions of the channel (9 Å *vs.* 80 × 80 $Å^2$; Hille, 1992; Li et al., 1994). Experiments with charged and uncharged lipid bilayers show that the composition does not affect metal ion induced shifts of activation and inactivation curves provided that the ionic strength is at least as high as it is in Ringer solution (Cukierman, 1991). Likewise, experimental evidence suggests that the charges of the attached carbohydrate chains play an insignificant role for gating of K channels. There is no correlation between metal ion induced shifts and putative glycosylation sites (Elinder, Madeja & Århem, 1996). Removal of glycosylation sites by mutagenesis does not affect the gating (Santacruz-Toloza et al., 1994; Talukder et al., 1994). For Na channels the results are conflicting. Experiments with neuraminidase that remove charged sialic residues from the carbohydrate chains have been reported both to shift (Recio-Pinto et al., 1990; Bennett et al., 1997) and not to shift (Frankenhaeuser, Ryan & Århem, 1976) the activation curve. However, the contribution of the sialic residues to the total functional surface charge was in the positive reports limited to about 25%. (The reported shift of 10 mV in physiological solutions indicates a 25% reduction in surface charge density, relatively independent of original density.)

Most surface charges affecting the gating thus seem to be confined to the channel protein itself in relatively high ionic strength solutions. In a previous investigation of five different K channel types expressed in *Xenopus* oocytes (Elinder et al., 1996) we found evidence for a positive correlation between the experimentally estimated charge densities and the net sum of the extracellularly located charged amino acid residues. However,

Correspondence to: P. Århem

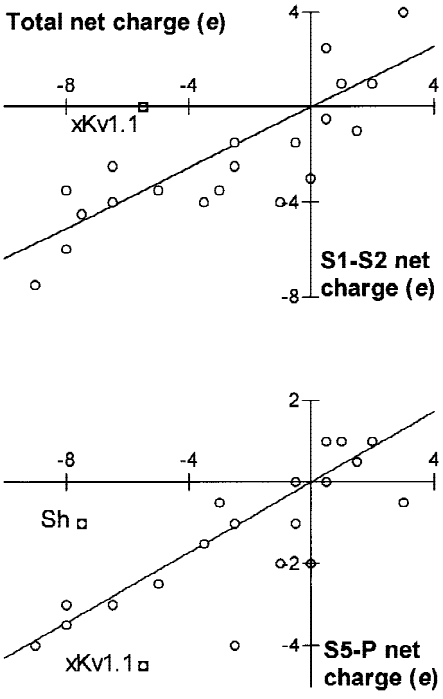

Fig. 1. Relation between total net charge (i.e., the net charge of the four extracellular loops) and net charge of the S1-S2 loop (upper panel) and of the S5-P loop (lower panel) for Kv channels. The charge values were calculated by assigning values of −1 to glutamate and aspartate, +1 to lysine and arginine and +0.5 to histidine. The amino acid sequences used are given in Gutman & Chandy (1995). The transmembrane segments were defined in the same way as in Gutman & Chandy (1995) except for the S1-S2 loop which included two extra residues at the N-terminal end (*see* Elinder & Århem, 1994a,b). Amino acid sequences of the S5-P loop for seven of the channels are in addition given in the following paper (Elinder et al., 1998). Continuous lines are least square fitted linear curves through the origin with slopes 0.64 (upper panel) and 0.43 (lower panel). Note that the diagram in the lower panel is close to that presented in Elinder et al., 1996).

the experimentally estimated charge densities also showed a positive correlation with the net charge of two of the extracellular loops; the loop between the transmembrane segments S1 and S2 (S1-S2) and that between S5 and the pore forming segment (S5-P). This is a consequence of the linear relationship between the net charge of these loops and the net charge of all the extracellular loops for the channels investigated (Kv1.1, 1.5, 1.6, 2.1 and 3.4).

Analyzing the relationship between the charge of the discussed extracellular loops for other cloned channels a pattern emerged. However, two channels were found to deviate from this pattern (*see* Fig. 1); xKv1.1 (from *Xenopus laevis*) and Shaker (from *Drosophila melanogaster*). Assuming that the S1-S2 loop is the main determinant, metal ions are predicted to cause a zero shift of the activation curve for xKv1.1 since this loop is uncharged (Fig. 1*A*). Assuming that the S5-P loop is the determinant, the metal ion induced shift is predicted to be considerable, since the S5-P loop of xKv1.1 is the most charged loop for any K channel (Fig. 1*B*). In contrast, the corresponding shift for the Shaker channel is predicted to be small, since the S5-P loop of this channel is relatively less charged than that of other K channels (Fig. 1*B*). This makes xKv1.1 and Shaker essential in an investigation of the location of the functional charge of voltage-gated channels.

In the present paper we have focused on the xKv1.1 channel. In a following paper we will describe the analysis of the Shaker K channel (Elinder, Liu & Århem, 1998). For the xKv1.1 channel we have analyzed effects of Mg^{2+} on one of the fast K channel types of *Xenopus* myelinated axons, here referred to as f_1/I channels [named f_1 in axons from *Rana esculenta* (Dubois, 1981), and I in axons from *Xenopus laevis* (Jonas et al., 1989)], assuming that this channel is identical with xKv1.1. There are strong reasons for such an assumption, presented in the Discussion. Given this identity, the node of Ranvier is an ideal preparation for the present study due to its accessibility for pharmacological substances and its good time resolution. The choice of Mg^{2+} was based on the assumption that it mainly screens the surface charges without binding, as suggested by other investigations (Hille, Woodhull & Shapiro, 1975; Cukierman & Krueger, 1990) as well as by the present study, and the following (Elinder et al., 1998).

Earlier estimations of surface charge densities of axonal *Xenopus* K channels have concerned the total population (Brismar, 1973; Elinder & Århem, 1994*a*,*b*). No attempt has been made to estimate the charge densities of the different K channel subpopulations separately before. Estimated values for the total population range from −0.34 to −0.6 elementary charges (e) nm^{-2}. In the present investigation we obtained a value for the f_1/I channel population of $-0.45\ e\ nm^{-2}$. Assuming that the f_1/I channel is identical to xKv1.1 (*see above*) the results suggest that the S5-P loop is the major determinant of the effective surface charges in voltage-gated K channels.

Materials and Methods

Electrophysiology

Large myelinated fibers were isolated from the sciatic nerve of unanesthetized decapitated toads of the species *Xenopus laevis.* Single fibers were mounted in a recording chamber and cut at half-internode length on both sides of the node under investigation. Vaseline seals were used to separate the electrolyte solutions. The chamber was connected by KCl bridges to the voltage-clamp apparatus. The chamber design, circuitry, and balancing procedures were essentially the same as described by Dodge & Frankenhaeuser (1958), with the modifications described by Århem, Frankenhaeuser & Moore (1973). To obtain good feedback control and recording situations, all experiments were performed at low temperature (8–10°C). Pulse generation and sampling were made us-

ing a TL-1 DMA interface and the pCLAMP software (Axon Instruments, Foster City, CA). Sampling interval was 50–200 μsec. The current calibration was based on the assumption of an axoplasmic resistance of 20 MΩ (half internode length). Leak currents were numerically subtracted from the recorded currents, assuming a linear behavior. The voltage clamp apparatus was designed to minimize amplification of voltage errors due to, for instance, stray capacitances and liquid junction potentials at the current clamp amplifier input. Other sources of error, such as the voltage drop over the series resistance of the nodal gap and differences in liquid junction potentials between the bridge solution and test solutions (*see* for instance Drouin & Neumcke, 1974), were predicted to be small and not corrected for.

The test solutions were applied to the pool with the node and consisted of $MgCl_2$ $6H_2O$ added to Ringer solution, consisting of (in mM): NaCl 115.5, KCl 2.5, $CaCl_2$ 2.0, and Tris buffer (adjusted to pH 7.2) 5.0. The solution used in the end pools consisted of (in mM): KCl 120.0 and Tris buffer (pH 7.2) 5.0.

Data Analysis

The effects of Mg^{2+} were analyzed in terms of effects on the open probability ($p_o(V)$) of the channels, estimated from the instantaneous value of the tail K current (I_K) at Na reversal potential (V_{Na}; about +40 mV) after 50–100 msec pulses to potentials between −100 and +60 mV from a holding potential of −100 mV (*see* protocol in Fig. 2). Due to initial oscillations of the tail I_K the instantaneous value used was extrapolated from later parts of the curve. The pulse duration used was found sufficient to give steady-state $p_o(V)$ values. Measurements at V_{Na} made I_K almost independent of $[K^+]_o$ and extracellular K^+ accumulation, because the expected inwardgoing K current is almost absent due to the lack of driving force (*c.f.* constant-field equation in Hodgkin & Katz, 1949; Frankenhaeuser, 1962). These conditions further made the Na current (I_{Na}) component of the instantaneous value negligible because of the small Na^+ driving force. Furthermore, the I_{Na} inactivation is almost complete at the end of the conditioning steps used. The Mg^{2+} effects were measured as shifts at the 25% level of maximum $p_o(V)$. At this part of the $p_o(V)$ curve (comprising the most negative potentials) only f_1/I channels are open (Dubois, 1981; Jonas et al., 1989; Bräu et al., 1990).

The analysis of the effects on fixed surface charges was based on the Grahame equation [modification of Eq. 40 in Grahame (1947)]

$$\sigma^2 = 2\varepsilon_r\varepsilon_0 RT\sum_{i=1}^{n} c_i(\exp(-z_i\psi_0 FR^{-1}T^{-1}) - 1), \quad (1)$$

where σ is the density of surface charges, ε_r is the dielectric constant of the medium, ε_0 is the permittivity of free space, c_i is the bulk concentration and z_i is the valence of *i*th ionic species, *n* is the number of ionic species, and ψ_0 is the surface potential. *T*, *R* and *F* have their usual thermodynamic meanings. The Grahame equation is based on the assumption of smeared charges. Theoretically it has been shown that this assumption can be used at charge densities more negative than −0.16 *e* nm^{-2} (Peitzsch et al., 1995). In the present investigation the charge density was found to be −0.45 *e* nm^{-2}, justifying the use of Eq. 1.

Results

Open Probability Curve and its Components

Figure 2 (middle panel) shows currents, evoked by a series of steps (upper panel) to various potentials in increments of 20 mV from a holding potential of −100 mV, followed after 55 msec by a step to +35 mV, which was close to V_{Na} in this axon. The leakage current was linearly subtracted and no capacitance compensation was used. The I_K depicted comprise currents mainly through the two fast channel types f_1/I and f_2/F (*see* Dubois, 1981; Jonas et al., 1989). The slow channel population s/S is negligible in this time range (*see* Bräu et al. (1990) for the validity of this assumption).

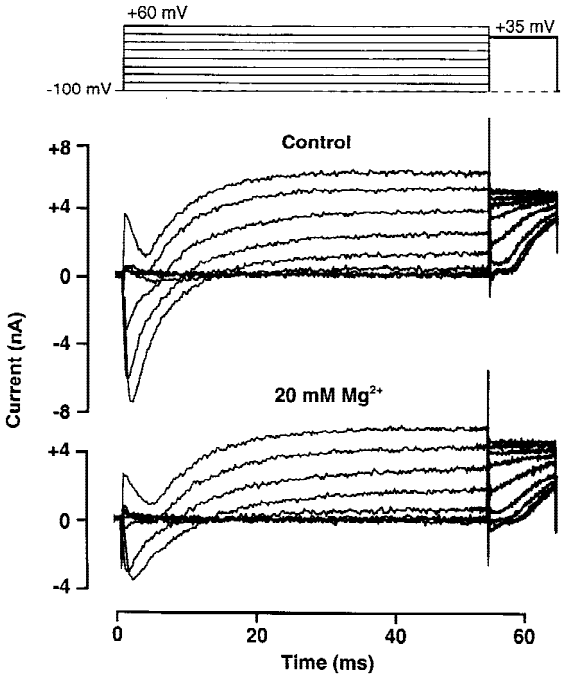

Fig. 2. Effect of 20 mM Mg^{2+} on ion currents, associated with rectangular potential steps from −100 to +60 mV (each step separated by 20 mV), followed by a step to +35 mV. Holding potential is −100 mV. Note the change in sampling frequency at about 50 msec.

Figure 3*A* shows the $p_o(V)$ curve directly obtained from measurements of the instantaneous current. We attempted to separate the two fast channel populations by fitting $p_o(V)$ curves to the sum of the two Boltzmann distributions by a least-square procedure (Dubois, 1981; Benoit & Dubois, 1986; Bräu et al., 1990; Corrette et al., 1991). The double Boltzmann curve used was:

$$p_o(V) = A_1/(1 + \exp((V - V_1)/k_1)) + A_2/(1 + \exp((V - V_2)/k_2)) \quad (2)$$

where A_1 and A_2 are the relative magnitudes of the two populations, V_1 and V_2 are the potentials at the midpoint values, *V* the test-step potential, and k_1 and k_2 the slope values. However, it was found impossible to consistently separate the two populations by this procedure. This is illustrated in Fig. 3*A* where two solutions to Eq.

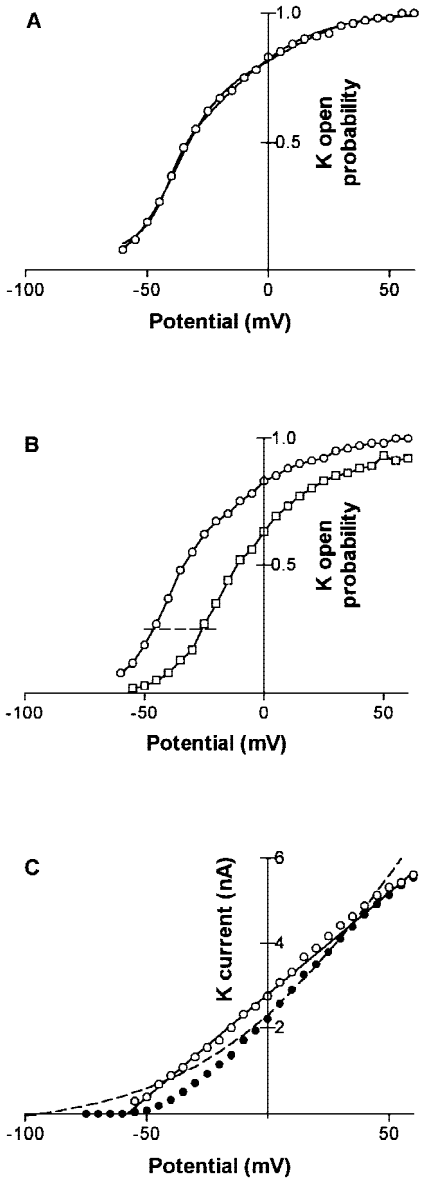

Fig. 3. Open probability $p_o(V)$ and steady-state current $I_K(V)$ curves for the *K* channels of the axon in Fig. 2. (*A*) The plotted values are normalized instantaneous currents after the end of the first test pulse in control solution, estimated as described in Materials and Methods. Continuous lines are least square fitted solutions to Eq. 2. A_1 and A_2 set either to 0.75 and 0.25, or to 0.25 and 0.75. Resulting values in the first case are $k_1 = 10.0$ mV, $k_2 = 13.4$ mV, $V_1 = -39$ mV and $V_2 = 10$ mV; in the second case $k_1 = 3.9$ mV, $k_2 = 19.7$ mV, $V_1 = -42$ mV, and $V_2 = -23$ mV. (*B*) Values in control (circles; same as in *A*) and in 20 mM Mg^{2+} solution (squares). Dashed line indicates the 0.25% level. The shift at this level was 20 mV. (*C*) Filled circles are $I_K(V)$ values. Open circles are steady-state $I_K(V)$ divided by $p_o(V)$ from (*A*). Continuous line is the least square fitted solution to the conductance equation $I_K(V) = G_K (V - V_K)$. $V_K = -58$ mV and $G_K = 49$ nS. Dashed line is the least square fitted solution to the constant-field equation (Hodgkin & Katz, 1949; Frankenhaeuser, 1962) for $[K^+]_i = 120.0$ mM and $[K^+]_o = 2.5$ mM. $P_K = 0.20\ 10^{-9}$ cm^3 sec^{-1}.

2 fitted to experimental $p_o(V)$ data are depicted, one with relative magnitudes (A_1 and A_2) of 0.75 and 0.25 and the other with relative magnitudes of 0.25 and 0.75 (other parameters being defined in the figure legend). Both solutions seem equally well fitted to the experimental data.

That the impossibility to separate the open probability curves for the two populations did not depend on the presently used measuring procedure *per se* was shown in experiments using other strategies. Thus we calculated $p_o(V)$ from measurements of the instantaneous value of tail currents at −70 mV in high $[K^+]_o$ solution (120.0 mM KCl). Under these conditions the measured currents are large and the extracellular K^+ accumulation low (Frankenhaeuser, 1962; Dubois, 1981). We also calculated $p_o(V)$ from measurements of steady state currents in Ringer or high $[K^+]_o$ solution. For this we assumed that $p_o(V)$ is directly proportional to conductance rather than to permeability which often has been used to describe open probability in the nodal membrane (Frankenhaeuser, 1962; *see* Hille, 1970). The reason for this somewhat controversial assumption is demonstrated in Fig. 3*C* showing the $I_K(V)$ relation for maximally open channels (open circles; the normal $I_K(V)$ curve is shown as filled circles). The relation is linear as predicted by the conductance equation (the solution to the constant-field equation is dashed line, *see* legend to Fig. 3). Similar results have been obtained by Dubois & Bergman (1977), and Bräu et al. (1990). In summary, the results from these supplementary experiments confirmed the conclusion that it is not possible to separate the open probability curves for the two fast K channel populations by the methods used.

However, by taking the different activation kinetics for the two channel types into account, it is possible to analyze the f_1/I channel separately. The f_1/I population is known to activate at much more negative potentials (midpoint of activation curve at about −50 mV) than the f_2/F population (midpoint at about −10 mV; Benoit & Dubois, 1986; Jonas et al., 1989; Bräu et al., 1990), implying that the $p_o(V)$ curve at the most negative potentials mainly reflects the activity of the f_1/I channels. In the following we therefore estimated the Mg^{2+} induced shift of the f_1/I channel open probability by measuring the shift at $p_o = 0.25$.

Effects of Mg^{2+}

Figure 2 (lower panel) shows effects of 20 mM Mg^{2+} on the nodal currents. Fig. 3*B* shows the corresponding $p_o(V)$ curve. The maximum $p_o(V)$ is reduced about 10% and the $p_o(V)$ curve is shifted in positive direction along the potential axis, the magnitude being 20 mV at $p_o = 0.25$. In analyzing the mechanism of this shift, it was assumed that the shift was mainly caused by screening of and not by binding to the surface charges. Necessary

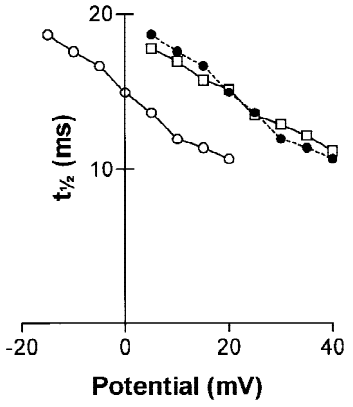

Fig. 4. Time to half-steady-state current ($t_{1/2}$) for the axon in Fig. 2. Values in control (circles) and in 20 mM Mg^{2+} solution (squares). Filled circles indicate the control values shifted by 20 mV.

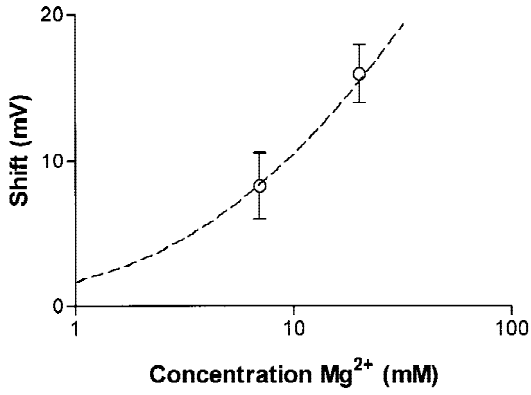

Fig. 5. Dependence of $p_o(V)$ shifts on Mg^{2+} concentration. Data from four axons (mean ± SEM). The dashed line is the least-square fitted solution to the Grahame equation (Eq. 1). The surface charge density obtained is −0.45 e nm^{-2}.

(but not sufficient) requirements for such an assumption are (i) that the shift of the steady state $p_o(V)$ curve equals the shift of the time constant *vs.* potential curve and (ii) that the shift is smaller than or equal to the shift caused by other divalent cations. Figure 4 shows the effect of 20 mM Mg^{2+} on the time to half steady state I_K ($t_{1/2}$). Only values up to +20 mV in control solution were considered because the f_2/F population interferes at more positive potentials (*see* Jonas et al., 1989). As seen the effect is a shift of about 20 mV in good agreement with the shift of the $p_o(V)$ curve, thus fulfilling the first requirement above. A similar effect has been shown for Sr^{2+} (Elinder et al., 1996). Concerning the second requirement it is known from other investigations (Hille et al., 1975; Cukierman & Krueger, 1990) that Mg^{2+} (together with another hard metal ion, Sr^{2+}) belongs to the group that causes the smallest shift of the $p_o(V)$ curve. Both requirements above thus support the view that the shift effect of Mg^{2+} mainly is a screening effect.

Estimation of Functional Surface Charge Density

Under the assumption of pure screening the functional charge density of the f_1/I channel can be estimated from the Grahame equation (Eq. 1). Figure 5 shows shifts of $p_o(V)$ curves at $p_o = 0.25$ for four axons. The dashed line is the least square fitted solution to the Grahame equation. The corresponding surface charge density is −0.45 e nm^{-2}. Although the shift values showed considerable variability, the corresponding charge densities systematically were higher than those of the K channels analyzed in the previous investigation (Elinder et al., 1996). The charge densities corresponding to the SEM bar for 20 mM Mg^{2+} in Fig. 5 range from −0.39 to −0.62 e nm^{-2}, while those of the channels in the previous investigation varied from −0.37 to −0.11 e nm^{-2}.

The Main Determinant of Functional Surface Charge Density

By comparing the surface charge density result with the data on the five Kv channels from the previous study (Elinder et al., 1996) we are now in the position to estimate the relative importance of the extracellular loops in determining the functional charge density. The results of the previous analysis suggested that either the S1-S2 or the S5-P loop or the combination of all extracellular loops determined the functional surface charge density. An analysis of the present results suggests that the S5-P segment is the major determinant. From Fig. 6 it is clear that the net charge of S5-P shows better correlation ($r^2 = 0.91$) with the experimentally estimated charge densities than the total net charges ($r^2 = 0.78$). The net charge of S1–S2 shows a less good correlation ($r^2 = 0.44$).

Discussion

The main experimental finding of the present investigation is that the fast K channel, activating at most negative potentials of the node of Ranvier in *Xenopus* axons (f_1/I) has a functional charge density of −0.45 e nm^{-2}. Such an estimation for a separate channel population separation has not been done before. Assuming that f_1/I in *Xenopus* is identical with xKv1.1 (at least with respect to charge profile) the results suggest that the S5-P loop constitutes a better determinant of the functional surface charge density for voltage-gated K channels than the other extracellular segments or the total surface net charge (*see* Fig. 6).

Molecular Identity of the f_1/I Channel

Several lines of evidence suggest that f_1/I is closely related to xKv1.1. Perhaps the strongest argument is ob-

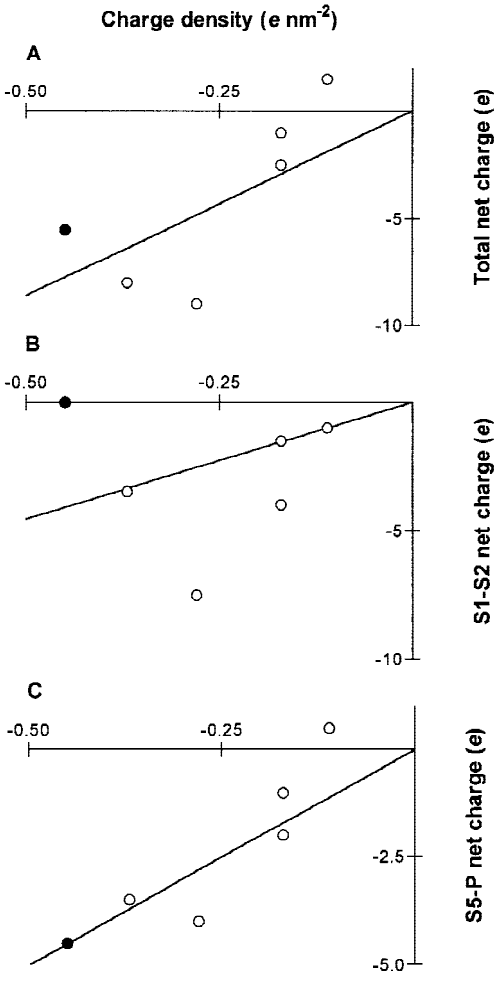

Fig. 6. Relation between experimentally obtained charge density and net charge of all extracellular loops (*A*), net charge of the S1-S2 loop (*B*), and net charge of the S5-P loop (*C*) for xKv1.1 (filled circles) and the Kv channels investigated in Elinder et al. (1996; unfilled circles). For definition of extracellular loops see legend to Fig. 1. Continuous lines are least square fitted linear curves through the origin. Slopes are 17.1 nm^2 (*A*), 9.1 nm^2 (*B*), and 10.1 nm^2 (*C*) and r^2 values 0.78 (*A*), 0.44 (*B*) and 0.91 (*C*).

tained from a comparison of pharmacological profiles. The f_1/I channel is blocked by tetraethylammonium (TEA) and dendrotoxin (DTX) with K_d values of about 1 mM and 10 nM respectively (Dubois, 1981; Benoit & Dubois, 1986; Bräu et al., 1990; Hille, 1992). Of cloned voltage activated channels only Kv1.1 (including xKv1.1) and Kv3.1–3.4 have K_d values in the range 0.1–1 mM for TEA, the other Kv channels having much higher K_d values (Table 3 in Gutman & Chandy, 1995). Concerning DTX only Kv1.1 (including xKv1.1) and Kv1.2 and Kv1.6 have K_d values in the nM range, the other Kv channels having much higher values (Table 3 in Gutman & Chandy, 1995). Further argument is provided by a comparison of activation potential ranges. The midpoint potential of the $p_o(V)$ curve for the f_1/I channel is about −50 to −40 mV. Of the Kv channels Kv1.1 (including xKv1.1) activates at most negative potentials (midpoint in the range −34 to −27 mV; Table 3 in Gutman & Chandy, 1995). The suggested similarity is also supported by a comparison of kinetics. The f_1/I channel shows noninactivation kinetics in similarity with Kv1.1 (including xKv1.1). It should also be noted that a high level of expressed mRNA of Kv1.1 is found in rat sciatic nerves (Beckh & Pongs, 1990). These arguments clearly suggest that f_1/I is of Kv1.1 type and thus probably identical to the Kv1.1 channel cloned from *Xenopus laevis*, i.e., xKv1.1.

Separation of Channel Populations

In the present investigation it was not possible to consistently separate the populations directly by an analysis of the $p_o(V)$ curve. This finding seems to differ from that of studies of *Rana esculenta* axons (Dubois, 1981; Benoit & Dubois, 1986), but also from that of other studies of *Xenopus laevis* (Bräu et al., 1990) and rat axons (Corrette et al., 1991). The reason for this difference is not clear. It might be related to species differences. The difference between the midpoints of the $p_o(V)$ curves of the two populations is smallest for rat (32 mV; Corrette et al., 1991), is slightly larger for *Xenopus laevis* (about 35 mV; Jonas et al., 1989; Bräu et al., 1990) and is largest for *Rana esculenta* (about 50 mV; Dubois, 1981; Benoit & Dubois, 1986).

It has been shown that the two populations can be pharmacologically separated by blocking the f_1/I population with dendrotoxin (Benoit & Dubois, 1986; Bräu et al., 1990). However, it is also known that the surface potential may affect the binding of toxins (Hurst et al., 1991; Escobar, Root & MacKinnon, 1993), making measurements of Mg^{2+} induced shifts uncertain. This was the reason why we did not use this separation method in the present investigation.

Conclusion

In conclusion, the present investigation excludes the extracellular loop between the S1 and S2 segments as determinant of the functional surface charge density and strengthens the view that the extracellular loop between the S5 and the pore-forming segments plays an essential role in this respect. Figure 6, however, shows that we cannot exclude the total net charge of the extracellular loops as a major determinant. As already suggested in the Introduction this can be critically tested by analyzing Mg^{2+} effects on the Shaker channel. This is done in the following paper (Elinder et al., 1998).

This work was supported by grants from the Swedish Medical Research Council (Project No. 6552), Karolinska Institutet, the Swedish Society for Medicine, and Hjärnfonden.

References

Århem, P., Frankenhaeuser, B., Moore, L.E. 1973. Ionic currents at resting potential in nerve fibers from *Xenopus laevis.* Potential clamp experiments. *Acta Physiol. Scand.* **88:**446–454

Beckh, S., Pongs, O. 1990. Members of the RCK family are differently expressed in the rat nervous system. *EMBO J.* **9:**777–782

Bennett, E., Urcan, M.S., Tinkle, S.S., Koszowski, A.G., Levinson, S.R. 1997. Contribution of sialic acid to the voltage dependence of sodium channel gating. *J. Gen. Physiol.* **109:**327–343

Benoit, E., Dubois, J.-M. 1986. Toxin I from the snake *Dendroaspis polylepis polylepis:* a highly specific blocker of one type of potassium channel in myelinated nerve fiber. *Brain Res.* **377:**374–377

Bräu, M.E., Dreyer, F., Jonas, P., Repp, H., Vogel, W. 1990. A K^+ channel in *Xenopus* nerve fibers selectively blocked by bee and snake toxins: binding and voltage-clamp experiments. *J. Physiol.* **420:**365–385

Brismar, T. 1973. Effects of ionic concentration on permeability properties of nodal membrane in myelinated nerve fibres of *Xenopus laevis.* Potential clamp experiments. *Acta Physiol. Scand.* **87:**474–484

Chandler, W.K., Hodgkin, A.L., Meves, H. 1965. The effect of changing the internal solution on sodium inactivation and related phenomena in giant axons. *J. Physiol.* **180:**821–836

Corrette, B.J., Repp, H., Dreyer, F., Schwarz, J.R. 1991. Two types of fast K^+ channels in rat myelinated nerve fibres and their sensitivity to dendrotoxin. *Pfluegers Arch.* **418:**408–416

Cukierman, S. 1991. Asymmetric electrostatic effects on the gating of rat brain sodium channels in planar lipid membranes. *Biophys. J.* **60:**845–855

Cukierman, S. 1993. Barium modulates the gating of batrachotoxin-treated Na^+ channels in high ionic strength solutions. *Biophys. J.* **65:**1168–1173

Cukierman, S., Krueger, B.K. 1990. Modulation of sodium channel gating by external divalent cations: differential effects on opening and closing rates. *Pfluegers Arch.* **416:**360–367

Dodge, F., Frankenhaeuser, B. 1958. Membrane currents in isolated frog nerve fiber under voltage clamp conditions. *J. Physiol.* **143:**76–90

Drouin, H., Neumcke, B. 1974. Specific and unspecific charges at the sodium channels of the nerve membrane. *Pfluegers Arch.* **351:**207–229

Dubois, J.-M. 1981. Evidence for the existence of three types of potassium channels in the frog ranvier node membrane. *J. Physiol.* **318:**297–316

Dubois, J.-M., Bergman, C. 1977. The steady-state potassium conductance of the Ranvier node at various external K-concentrations. *Pfluegers Arch.* **370:**185–194

Elinder, F., Århem, P. 1994*a*. Effects of gadolinium on ion channels in the myelinated axon of *Xenopus laevis:* four sites of action. *Biophys. J.* **67:**71–83

Elinder, F., Århem, P. 1994*b*. The modulatory site for action of gadolinium on surface charges and channel gating. *Biophys. J.* **67:**84–90

Elinder, F., Liu, Y., Århem, P. 1998. Divalent ion effects on the Shaker K channel suggest a pentapeptide sequence as determinant of functional surface charge density. *J. Membrane Biol.* **165:**183–189

Elinder, F., Madeja, M., Århem, P. 1996. Surface charges of K channels. Effects of strontium on five cloned channels expressed in *Xenopus* oocytes. *J. Gen. Physiol.* **108:**325–332

Escobar, L., Root, M.J., MacKinnon, R. 1993. Influences of protein surface charges on the bimolecular kinetics of a protein channel peptide inhibitor. *Biochemistry* **32:**6282–6297

Frankenhaeuser, B. 1962. Potassium permeability in myelinated nerve fibers of *Xenopus laevis. J. Physiol.* **160:**54–61

Frankenhaeuser, B., Hodgkin, A.L. 1957. The action of calcium on the electrical properties of squid axons. *J. Physiol.* **137:**218–244

Frankenhaeuser, B., Ryan, K., Århem, P. 1976. The effects of neuraminidase and protamine chloride on potential clamp parameters of the node of Ranvier. *Acta Physiol. Scand.* **96:**548–557

Grahame, D.C. 1947. The electrical double layer and the theory of electrocapillarity. *Chemical Review* **41:**441–501

Gutman, G.A., Chandy, K.G. 1995. Voltage-gated K^+ channels. *In:* Handbook of Receptors and Channels. Ligand- and Voltage-Gated Ion Channels. R.A. North, editor. pp. 1–71. CRC Press, Boca Raton

Hille, B. 1970. Ionic channels in nerve membranes. *Prog. Biophys. Mol. Biol.* **21:**1–32

Hille, B. 1992. Ionic channels of excitable membranes. pp. 612. Sinauer, Sunderland, MA

Hille, B., Woodhull, A.M., Shapiro, B.I. 1975. Negative surface charge near sodium channels of nerve: divalent ions, monovalent ions, and pH. *Phil. Trans. R. Soc. London B* **270:**301–318

Hodgkin, A.L., Katz, B. 1949. The effect of sodium ions on the electrical activity of the giant axon of the squid. *J. Physiol.* **108:**37–77

Hurst, R.S., Bush, A.E., Kavanaugh, M.P., Osborne, P.B., North, R.A., Adelman, J.P. 1991. Identification of amino acid residues modified in dendrotoxin block of rat voltage dependent potassium channels. *Mol. Pharmacol.* **40:**572–576

Jonas, P., Bräu, M.E., Hermsteiner, M., Vogel, W. 1989. Single-channel recording in myelinated nerve fibers reveals one type of Na channel but different K channels. *Proc. Nat. Acad. Sci. USA* **86:**7238–7242

Li, M., Unwin, N., Stauffer, K.A., Jan, Y.N., Jan, L.Y. 1994. Images of purified Shaker potassium channels. *Curr. Biol.* **4:**110–115

McLaughlin, S. 1989. The electrostatic properties of membranes. *Ann. Rev. Biophys. Chem.* **18:**113–136

Peitzsch, R.M., Eisenberg, M., Sharp, K.A., McLaughlin, S. 1995. Calculation of the electrostatic potential adjacent to model phospholipid bilayers. *Biophys. J.* **68:**729–738

Recio-Pinto, E., Thornhill, W.B., Duch, D.S., Levinson, S.R., Urban, B.W. 1990. Neuraminidase treatment modifies the function of electroplax sodium channels in planar lipid bilayers. *Neuron* **5:**675–684

Santacruz-Toloza, L., Huang, Y., John, S.A., Papazian, D. 1994. Glycosylation of Shaker potassium channel protein in insect cell culture and in *Xenopus* oocytes. *Biochemistry* **33:**5607–5613

Talukder, G., Gibbons, S.J., Tamkun, M.M., Harrison, N.L. 1994. Probing the site of Zn^{2+} action using cloned and mutant voltage-gated K^+ channels. *Biophys. J.* **66:**A209 (*Abstr.*)